Constraint relaxation leads to jamming

Eial Teomy [1] and Yair Shokef [1,2]
[1] *School of Mechanical Engineering, Tel Aviv University, Tel Aviv 69978, Israel*
[2] *Sackler Center for Computational Molecular and Materials Science, Tel Aviv University, Tel Aviv 69978, Israel*

(Received 18 August 2020; accepted 11 December 2020; published 31 December 2020)

Adding transitions to an equilibrium system increases the activity. Naively, one would expect this to hold also in out-of-equilibrium systems. We demonstrate, using relatively simple models, how adding transitions to an out of equilibrium system may in fact reduce the activity and even cause it to vanish. This surprising effect is caused by adding heretofore forbidden transitions into less and less active states. We investigate six related kinetically constrained lattice gas models, some of which behave as naively expected while others exhibit this nonintuitive behavior. These models exhibit an absorbing state phase transition, which is also affected by the added transitions. We introduce a semi-mean-field approximation describing the models, which agrees qualitatively with our numerical simulation.

DOI: 10.1103/PhysRevE.102.062155

I. INTRODUCTION

For an equilibrium system, adding more transitions to its state space increases the activity. More generally, this holds for any system in which the steady-state distribution is not affected by the added transitions. In contrast, adding transitions in systems that are out of equilibrium may either increase or decrease the activity. Consider, for example, the directed percolation model [1] with additional dynamics that allow removal or addition of active sites. Adding such a transition decreases (for removal) or increases (for addition) the activity, and this change is predicted even on the mean-field (MF) level. Naively, one would expect that the MF prediction holds qualitatively, i.e., whether the activity is increased or decreased by the additional transition. However, as we show here, adding transitions that increase the activity at the MF level may in fact decrease the overall activity of the system, and in extreme cases may even attract the system to an absorbing state which was inaccessible before adding the transitions. Conceptually, this is similar to several phenomena seen in many-particle out-of-equilibrium systems, such as the faster-is-slower effect [2–6], slower-is-faster effect [7,8], and motility-induced phase separation [9–16], in which the total activity decreases as the activity of the individual particles increases.

Consider for example an ergodic system in equilibrium, depicted in Fig. 1(a). A concrete example of such a system is the symmetric exclusion process [17], which is a lattice gas in which each particle may hop to a neighboring site if the target site is vacant. Removing transitions and their reciprocal transition keeps the system in equilibrium [Fig. 1(b)], but may cause it to become nonergodic [Fig. 1(c)]. A class of models which demonstrate this is kinetically constrained models (KCMs) [18–28], in which a particle may hop to a neighboring site if the target site is vacant, and the neighborhood of the particle satisfies some model-dependent rule, both before and after the move. These models obey detailed balance, since by construction if a transition is allowed, its reverse is also allowed at the same rate. Essentially, adding this kinetic constraint removes some of the bonds from the transition graph of Fig. 1(a) and transforms the system into the one schematically illustrated in Fig. 1(b). At high enough particle density, these models become nonergodic, as schematically depicted in Fig. 1(c). KCMs were originally introduced in order to explain the kinetic origins of the glass or jamming transitions [19,29]. However, more recently, they have been demonstrated to be interesting on their own right as statistical mechanics models for nonequilibrium situations [30–32].

When one-way transitions are added to the system, it is driven out of equilibrium, as shown for instance in going from Figs. 1(b) to 1(d). In KCMs, this corresponds to allowing some of the moves which are prohibited by the kinetic constraint, but not their reverse moves. If the original KCM is ergodic, these additional one-way transitions increase the activity in the system, as is the case in going from Figs. 1(b) to 1(d). However, if the original KCM is nonergodic, these additional one-way transitions may create a path into absorbing states and decrease the long time activity in the system, as is the case when going from Figs. 1(c) to 1(e). In less extreme cases, these additional transitions may lead the system into a region in state space which contains less active states, and thus reduce the activity without reaching an absorbing state. Another way to add transitions is connecting the system to external reservoirs [30,32–36]. Such a system with a finite number of states will eventually reach one of the absorbing states, and thus its steady state contains only the absorbing states, and so its activity is zero. However, in the infinite-size limit an absorbing-state phase transition appears [37–39] as a function of some control parameter, such as the density of particles. As the system size increases, below the critical density the time to reach the absorbing states becomes exponentially large in the system size, such that in the infinite-size limit the steady state contains nonabsorbing states and the activity is finite. Above the critical density, the time to reach an absorbing state is finite even in the infinite-size limit, and thus the steady-state activity is zero. It is possible that the time

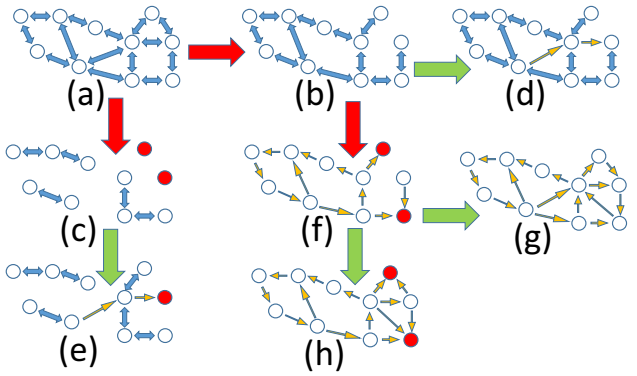

FIG. 1. A sketch of discrete dynamical systems and the transitions between their states: (a), (b) Ergodic equilibrium systems, (c) a system which obeys detailed balance but is not ergodic, (d)–(h) nonequilibrium systems violating detailed balance. The big red arrows between systems represent a removal of transitions, and the big green arrows represent an addition of transitions. In each system, absorbing states are denoted by a red circle, two way transitions by a blue double-sided arrow, and one-way transitions by an orange arrow.

to reach the steady state becomes algebraically large as the system size increases, and in this case it is possible that in the infinite-size limit the system never reaches the absorbing state, but also does not reach any other steady state. A trivial example is a simple random walker with absorbing boundary conditions.

Another way to drive dynamical systems out of equilibrium is to make all transitions one-way only, as shown in going from Figs. 1(b) to 1(f). This transformation might turn the long time activity to zero, but not necessarily. In lattice gases, this can be achieved by allowing the particles to move only in one direction [17,40]. Adding one-way transitions to this system may increase the activity [Fig. 1(g)] or decrease it [Fig. 1(h)]. In extreme cases, either adding or removing transitions may cause some states to become absorbing and jam the system, i.e., cause the long-time activity to become zero, or cause some absorbing states to become nonabsorbing and unjam the system, i.e., increase the long-time activity from zero to a finite value. In this paper we investigate such extreme behavior and provide concrete examples for this nonintuitive result. A less extreme method is to break detailed balance by biasing the particles to move in a certain direction [41–48].

We consider six related modified KCMs, one of which is the equilibrium Kob-Andersen (KA) model [49], and the others are out of equilibrium variants of it, which add or remove one-way transitions. By investigating these models numerically, we demonstrate how in some cases adding transitions that increase the activity at the MF level also increases the activity in the system, while in other cases it counterintuitively decreases the activity and may even jam the system. We also derive a semi-mean-field (SMF) analytical approximation for the activity, and we demonstrate how it qualitatively captures the behavior that we observe numerically for the different models. Although the models we consider here are relatively simple, our results can be generalized to other, more complicated systems driven out of equilibrium by adding transitions. The models are described in Sec. II, and their activity is investigated in Sec. III. Section IV concludes the paper. The technical derivations of our results are presented in the Appendixes.

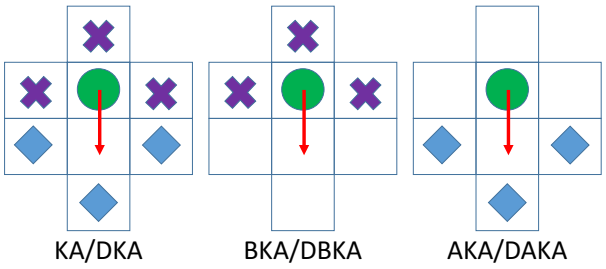

FIG. 2. An illustration of the kinetic constraints for a particle (green circle) moving to one of its nearest neighbors. The three sites marked by a purple × are the Before group, and the three sites marked by a blue ◇ are the After group. In the KA and DKA models at least one of the sites in the Before group and at least one of the sites in the After group need to be vacant in order for the particle to move. In the BKA and DBKA models only the Before group is checked, while in the AKA and DAKA models only the After group is checked.

II. THE MODELS

In this paper we consider six related models. The first model, from which all the others are derived, is the KA KCM on a 2D square lattice. In this model, a particle can hop to one of its four neighboring sites if that site is vacant and if both before and after the move at least two of the particle's four neighbors are vacant; see Fig. 2(a). This model obeys detailed balance with respect to a trivial Hamiltonian; for each allowed move, also the reverse move is allowed and at the same rate. In the steady state, the occupancy of all states is equal and there are no probability currents between the states of the system. In the infinite-size limit the KA model is always ergodic, while in finite systems it jams at some size-dependent density due to finite-size effects [50–53]. In a system of size $L \times L$, the critical density in the KA model is given by $\rho_c^{\mathrm{KA}}(L) = 1 - \lambda(L)/\ln L$, where $\lambda(L)$ depends weakly on L, converges to $\pi^2/18 \approx 0.55$ in the $L \to \infty$ limit, and is approximately $\lambda(L) \approx 0.25$ for all system sizes considered in this paper [53,54].

A system is jammed when it contains particles that will never be able to move, while an unjammed system does not. Note that if a particle cannot move at the current configuration, but will be able to move if some other particles move, then the system is not jammed. For example, the particles marked by an empty circle in Fig. 3 will never be able to move no matter how the three particles marked with a green circle and a purple × move, and therefore the system depicted there is jammed. We define the activity as the number of moves per unit time, and thus a jammed system may still be active if some of the particles in it can move.

We now define two variants of the KA model, namely, the After-KA (AKA) and the Before-KA (BKA) models. In the AKA (BKA) model, a particle can hop to an adjacent vacant site if after (before) the hop at least two of its four neighbors are vacant; see Figs. 2(b) and 2(c). As opposed to the KA

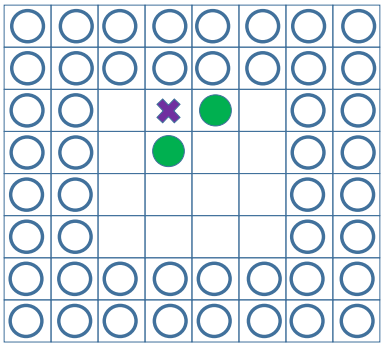

FIG. 3. An illustration of rattlers trapped inside a cage in the KA or BKA models. The particles on the edges (empty circles) are permanently frozen since at least three of their nearest neighbors are occupied by other permanently frozen particles. Although the × particle cannot currently move, it will be able to after the particles marked with a solid green circle move.

model, the AKA (BKA) model allows a particle to move regardless of the occupancy of the neighbors before (after) the move. Hence these two models both allow all the moves of the KA model as well as additional moves. These two models are out of equilibrium, since some transitions, namely, some of those that are prohibited in the KA model, are allowed here but their inverse transitions and not.

The last three models we consider are the driven variants of the three aforementioned models, which we call the DKA, DAKA, and DBKA models, where the D stands for driven. In these driven models all particles can move only along one of the four directions, which we designate as down. For such a move to occur the same kinetic constraints are required to hold as in the KA, AKA, and BKA models, respectively. The DKA model was recently investigated numerically [31], and it was found that this model has an absorbing state phase transition such that the steady-state current vanishes beyond a certain nontrivial critical density. Similar results were found for a variant of the KA model in which the particles can move in all four directions, but are biased in a particular direction [46,48].

III. ACTIVITY

A. Definition and mean-field approximation

In this section we investigate the activity in the system after it had reached the steady state. We define the activity, K, as the number of moves per unit time per lattice site. In the driven models it is equal to the current, and it may be written as $K = \rho P_{\rm F}$, where ρ is the fraction of occupied sites and $P_{\rm F}$ is the probability that a given particle can move downwards. In general the activity is equal to

$$K = \frac{\rho}{d}\sum_{n=1}^{4} n P_{{\rm F,n}}, \tag{1}$$

where $P_{\rm F,n}$ is the fraction of particles that can move in n of the four directions, and d is the number of allowed directions for motion, with $d = 1$ in the driven models and $d = 4$ in the undriven models. Note that while an undriven system may be jammed, i.e., that a finite fraction of the particles are permanently frozen and will never be able to move whatever the future dynamics of the system may be, there could still be rattlers, which are particles able to move back and forth inside a confined space, and thus the activity does not vanish in those cases. See Fig. 3 for an illustration of such a case.

We start by considering a mean-field (MF) approximation of the activity, in which we ignore all correlations between occupancies of neighboring sites. This approximation is exact in the KA model, for which there are no correlations [49]. The MF approximation for the activity in the various models is

$$\begin{aligned} K_{\rm MF}^{\rm KA} &= K_{\rm MF}^{\rm DKA} = \rho(1-\rho)(1-\rho^3)^2, \\ K_{\rm MF}^{\rm AKA} &= K_{\rm MF}^{\rm BKA} = K_{\rm MF}^{\rm DAKA} = K_{\rm MF}^{\rm DBKA} \\ &= \rho(1-\rho)(1-\rho^3). \end{aligned} \tag{2}$$

For the KA and DKA models, the terms on the right-hand side correspond respectively to the probabilities that a site is occupied, that its neighbor in the chosen direction of motion is vacant, and that at least one of the three sites both in the Before and the After group is vacant. In the BKA and DBKA (AKA and DAKA) models, the last term correspond to the probability that at least one of the three sites in the Before (After) group is vacant. Note that under the MF approximation there is no difference between the driven and undriven models, and furthermore the AKA and BKA have the exact same MF behavior. Also note that the MF activity in the KA model is lower than the MF activity for the AKA and BKA models, due to the extra constraint in the KA model. The MF activity is finite for all densities and vanishes only either when $\rho = 0$ and there are no particles that can move and contribute to the activity, or when $\rho = 1$ and the system is fully occupied such that there are no vacant sites that particles can move into.

However, as we will show below numerically and semianalytically, each of the five nonequilibrium models exhibits an absorbing state phase transition with a finite, nontrivial critical density above which the activity in the steady state vanishes. We now derive a SMF approximation for the activity, which considers some of the correlations in the system, and then we will compare it to simulation results. Our SMF approximation predicts a finite, nontrivial value for the critical density at which the activity vanishes and thus qualitatively captures the simulation results. However, the SMF approximation does not capture the numerical values of the critical densities in the different models.

B. Semi-mean-field approximation

We describe here a sketch of the SMF approximation for the driven models, with the full details given in the Appendixes. It is straightforward, yet more lengthy to follow the same steps and obtain the SMF approximation also for the undriven models. In the SMF approximation for the driven models, at any moment in time we divide all particles into three groups: free (F), jammed (J), and blocked (B). The particles in the free group are those that can move. The particles in the jammed group are those that have a vacancy in the site below them, but cannot move in their next step solely due to the kinetic constraint. The particles in the blocked group are those whose neighboring site in the direction of the flow is occupied and therefore cannot move regardless of the kinetic constraint. We denote the fractions of particles in the free,

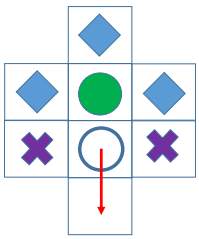

FIG. 4. An illustration of the transition from a blocked state to a free state in the DBKA model. The main particle whose state changes in marked by a full green circle, and the blocking particle by an empty circle. At least one of the × sites needs to be vacant in order for the blocking particle to move, and at least one of the ⋄ sites needs to be vacant in order for the main particle to be free after the blocking particle moves.

jammed, and blocked groups by P_{F}, P_{J}, and P_{B}, respectively, where by construction

$$P_{\mathrm{F}} + P_{\mathrm{J}} + P_{\mathrm{B}} = 1. \tag{3}$$

Now we write a master equation for the rates for each particle to change its type

$$\frac{\partial P_\alpha}{\partial t} = \sum_{\beta\neq\alpha} r_{\beta,\alpha} P_\beta - \sum_{\beta\neq\alpha} r_{\alpha,\beta} P_\alpha, \tag{4}$$

where $\alpha, \beta = \mathrm{F}, \mathrm{J}, \mathrm{B}$ and $r_{\alpha,\beta}$ is the rate in which a particle of type α changes into a particle of type β. The rates themselves depend on P_{F} such that Eq. (4) represents a set of three coupled nonlinear equations, which may be reduced to two equations using Eq. (3). In order to find an approximation for the rates, we assume that each site not accounted for in the type of the state before the transition is occupied with probability ρ, and that within each group the probability to be in each of the microscopic states is proportional to its uncorrelated probability.

For example, consider the rate $r_{\mathrm{B,F}}$ in the DBKA model illustrated in Fig. 4. The configuration before the transition consists of the blocked particle and the blocking particle below it. In order for the blocked particle to change its type to a free particle, two independent conditions should be satisfied. First, the blocking particle needs to move. The blocking particle can move only if it is free itself. The kinetic constraint for the blocking particle to be free is that at least one of the three adjacent sites, except the site below it, is vacant. Since the site above it is occupied by the blocked particle, we approximate the probability that the blocked particle is free given that the site above it is occupied by the uncorrelated fraction of free sites with one of the three neighbors occupied, i.e., $(1-\rho^2)/(1-\rho^3)$. Note that if the blocking particle is free, the site below it must be vacant, and therefore the probability that it is vacant is already included in the probability that the blocking particle is free. The second condition for the blocked particle to change its type to a free particle is that at least one of its three other neighbors is vacant, the probability of which we approximate by $1-\rho^3$. Altogether, the rate $r_{\mathrm{B,F}}$ in the DBKA model is given by

$$r_{\mathrm{B,F}} = P_{\mathrm{F}} \frac{1-\rho^2}{1-\rho^3}(1-\rho^3) = (1-\rho^2)P_{\mathrm{F}}. \tag{5}$$

The other rates are generated in a similar fashion for the three driven models, as detailed in Appendix A.

For all six models, the rates $r_{\mathrm{B},\alpha}$ and $r_{\mathrm{J},\alpha}$ are proportional to P_{F} since they involve the movement of a particle besides the blocked or jammed main particle, and the rates $r_{\mathrm{F},\alpha}$ are linear in P_{F}, since they contain terms which correspond to the movement of the main particle and to movement of other particles. Therefore, we may write the rates as

$$\begin{aligned} r_{\mathrm{B},\alpha} &= \omega_{\mathrm{B},\alpha} P_{\mathrm{F}}, \\ r_{\mathrm{J},\alpha} &= \omega_{\mathrm{J},\alpha} P_{\mathrm{F}}, \\ r_{\mathrm{F},\alpha} &= \Omega_{\mathrm{F},\alpha} + \omega_{\mathrm{F},\alpha} P_{\mathrm{F}}, \end{aligned} \tag{6}$$

with $\omega_{\alpha,\beta}$ and $\Omega_{\alpha,\beta}$ depending only on the density, and obviously different for the six different models.

We now look for stationary solutions of Eq. (4) under the condition $0 \leqslant P_{\mathrm{F}}, P_{\mathrm{J}}, P_{\mathrm{B}} \leqslant 1$. The solution $P_{\mathrm{F}} = 0$ is always a stationary solution. We analytically find that if there is another stationary solution with $P_{\mathrm{F}} > 0$, then it is unique and given by

$$P_{\mathrm{F}} = \frac{(\Omega_{\mathrm{F,B}} + \omega_{\mathrm{J,B}})(\omega_{\mathrm{B,F}} - \omega_{\mathrm{J,F}}) - (\omega_{\mathrm{B,F}} + \omega_{\mathrm{B,J}} + \omega_{\mathrm{J,B}})(\Omega_{\mathrm{F,B}} + \Omega_{\mathrm{F,J}} - \omega_{\mathrm{J,F}})}{(\omega_{\mathrm{F,B}} + \omega_{\mathrm{F,J}})(\omega_{\mathrm{B,J}} + \omega_{\mathrm{J,B}}) + (\omega_{\mathrm{B,J}} + \omega_{\mathrm{F,B}})\omega_{\mathrm{J,F}} + \omega_{\mathrm{B,F}}(\omega_{\mathrm{F,J}} + \omega_{\mathrm{J,B}} + \omega_{\mathrm{J,F}})}. \tag{7}$$

In Appendix B we derive Eq. (7) and analytically show that if this solution exists, it is also stable. In Appendix C we analytically investigate the stability of the $P_{\mathrm{F}} = 0$ state under the SMF approximation, and find that for large enough P_{B}, the solution is stable.

For the three driven models, as well as for the BKA model, we numerically find that within the SMF approximation there is some finite, model-dependent critical density $0 < \rho_c < 1$ such that for densities higher than the critical density $\rho > \rho_c$, solving Eq. (7) yields a negative P_{F} and thus it does not exist, while for $\rho < \rho_c$ we find that $P_{\mathrm{F}} > 0$. Therefore, the critical density is defined as the solution to Eq. (7) with $P_{\mathrm{F}} = 0$. The critical densities we get from this SMF approximation are $\rho_{\mathrm{DKA}}^{\mathrm{SMF}} = 0.792$, $\rho_{\mathrm{DAKA}}^{\mathrm{SM}} = 0.933$, $\rho_{\mathrm{DBKA}}^{\mathrm{SMF}} = 0.679$, and $\rho_{\mathrm{BKA}}^{\mathrm{SMF}} = 0.858$.

In the driven models, the SMF approximation involves three different states. In the undriven models, we need to account for whether in each of the four directions the particle is free to move, blocked or jammed, which gives a total of $3^4 = 81$ states, which reduce to 20 by rotational and inversion symmetry. In the BKA model, however, the number of states is reduced to six, since a particle is jammed in a certain direction only if it is blocked in the other three directions. We therefore present in Appendix D also the analytical derivation of the SMF activity in the BKA model. We leave the derivation of the AKA and KA models, which are straightforward but

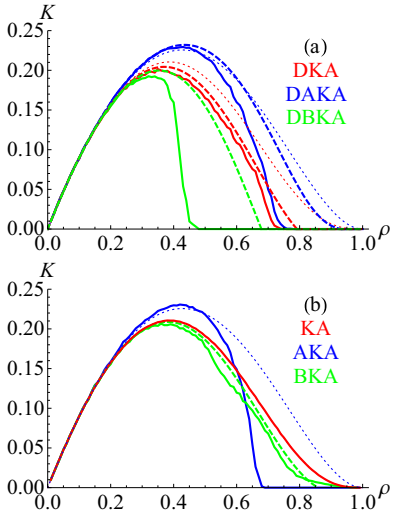

FIG. 5. Activity as a function of density for the three driven models (a) and the three undriven models (b), both from simulations results (continuous lines) and under the MF (dotted) and SMF (dashed) approximations. Note that the MF approximation is identical for the AKA/BKA/DAKA/DBKA models.

cumbersome, to future publications. However, we expect that the SMF approximation in the KA model would yield the exact same result as the MF approximation for that model since by construction it has no correlations. Thus, it would only be interesting to develop the SMF approximation for the AKA model.

C. Numerical results

We simulated the six models on a 30×30 lattice with periodic boundary conditions. For each density we averaged over 100 realizations, which start from different random initial conditions. We also performed simulations on larger systems up to 100×100 (not shown) and found very small deviations due to finite-size effects [50–53]. Figure 5 compares the steady-state activity evaluated from the simulations, the MF approximation and the SMF approximation. The SMF approximation overestimates the activity in the simulations for all six models. While the KA, DKA, AKA and DAKA models numerically converge to the steady state rather rapidly, the BKA and DBKA models converge very slowly for an intermediate range of densities ($0.37 < \rho < 0.43$ for the DBKA model and $0.50 < \rho < 0.81$ for the BKA model), as shown in Fig. 6.

We also measure in the simulations a lower bound on the fraction of frozen particles, P_Z, i.e., those that will never be able to move. For a given configuration, we do this by an iterative culling procedure [23,55]. This procedure starts by removing all mobile particles. In this new configuration, some particles which could not move before can now move, and we remove them too. We continue this procedure until all the remaining particles, if any, cannot be removed. This procedure gives a lower bound, since any particle which remains after this process is necessarily a frozen particle, but it is possible that some frozen particles have been removed [55]. Note that this procedure is not done during the dynamics, but on a snapshot of the system after it reaches the steady state. Except for the BKA model which did not reach the steady state at intermediate densities ($0.5 < \rho < 0.81$), we numerically find from Fig. 7 that P_Z jumps from 0 to 1 at some critical density. This critical density is the same one at which the activity vanishes, since zero activity implies $P_Z = 1$. Technically, since these are finite-size systems, the real steady state of the system is an absorbing state with zero activity, while the steady state we see in the simulations is a long-lived metastable state that will eventually reach the absorbing state. However, the lifetime of this metastable state grows with the system size, such that we expect that in the infinite-size limit it would be infinite, and the steady-state activity of the system would be finite. We conjecture that in the AKA, DKA, and DAKA models the life time of the metastable state increases exponentially with system size below the critical density, while in the BKA and DBKA models there is a range of densities for which the life time of the metastable state increases with the system size, but slower than exponentially, such that the activity in the system will decrease continuously but never vanish.

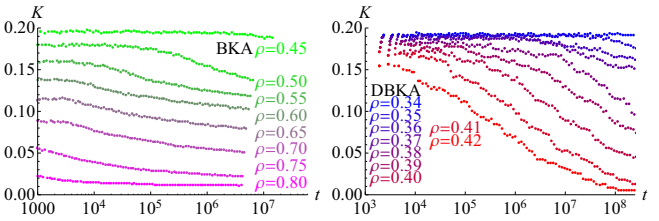

FIG. 6. Activity K as a function of time for the BKA and DBKA models for different densities, as obtained from numerical simulations.

Note that the critical density of the KA model in a system of size 30×30 is $\rho_c^{\mathrm{KA}}(30) \approx 0.93$ [53], much higher than the numerically obtained critical densities of the other five models studied here. This is in contrast to the MF approximation, which predicts $\rho_c^{\mathrm{KA}} = 1$. However, as stated above, the finite value of the critical density in the KA model is strictly a well understood finite-size effect, unrelated to the dynamically unreachable absorbing state, which does not affect significantly the critical densities of the other five models. In order to better understand the behavior of the different models, we present in Fig. 8 typical configurations of a 50×50 system after a very long time, as obtained from numerical simulations. In

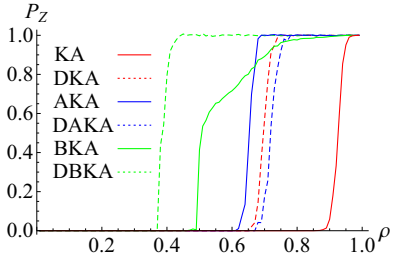

FIG. 7. Lower bound on the fraction of frozen particles, P_Z, as a function of density ρ after a very long time, as obtained from numerical simulations. Note that in the BKA model in the density range $0.5 < \rho < 0.81$, the system did not yet reach the steady state.

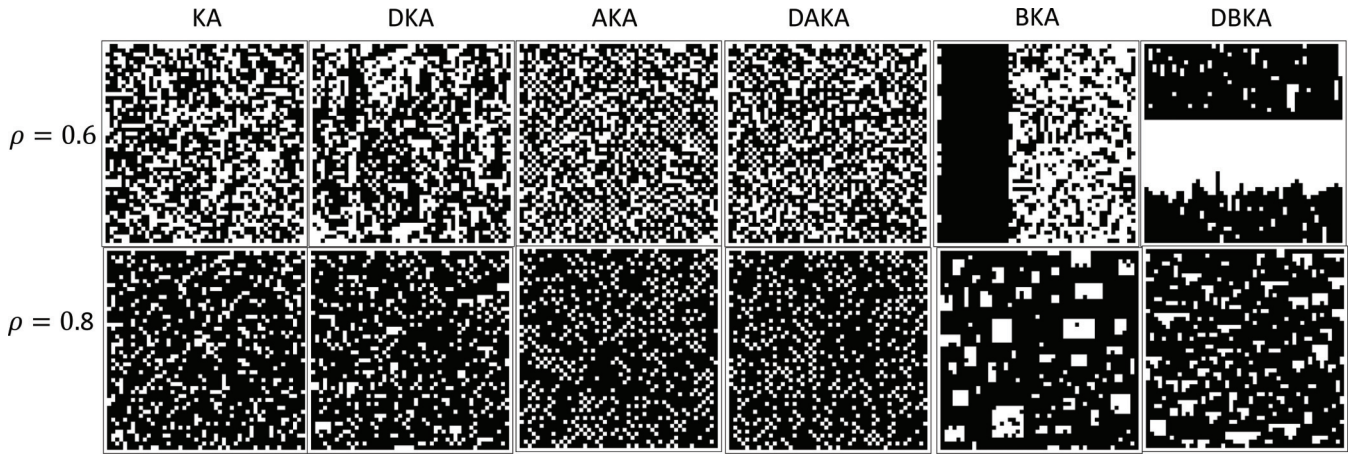

FIG. 8. A snapshot of 50×50 systems obtained from numerical simulations after a long time at density $\rho = 0.6$ (top) and $\rho = 0.8$ (bottom), for six models.

the KA, DKA, AKA, DAKA, and DBKA models the system has reached the steady state, while in the BKA it has not.

In the KA model, the system is always in equilibrium and there are no correlations between the occupancies of the sites. In the DKA model, the system is jammed at $\rho = 0.8$ and there are scattered structures of vacancies. At $\rho = 0.6$ the system is not jammed, but these structures can still be seen. These structures have been investigated in Refs. [31,48]. The AKA and DAKA models appear very similar. At $\rho = 0.8$ the system is jammed, and the vacancies tend to be arranged in a checkerboard pattern. At $\rho = 0.6$ the system is not jammed, but there are jammed regions with a checkerboard pattern. These checkerboard patterns are the sparsest locally jammed structures in the AKA and DAKA models, and due to their symmetry may be extended indefinitely. Hence, once a checkerboard pattern appears it is unstable only at its boundary. However, above the critical density the accumulation of particles at its boundary does not allow the pattern to break, but rather causes it to grow.

The behavior of the BKA model and the DBKA model is more interesting. Before investigating the configurations, we note that any particle that is part of two consecutive full rows is permanently frozen, since it is blocked in three directions and jammed in the other direction. In the KA, DKA, AKA, and DAKA models such a configuration cannot be generated dynamically, since a particle is prohibited from completing the second row. However, in the BKA and DBKA models such a configuration can be generated dynamically. At high densities in the DBKA model the system is jammed, and there are structures of vacancies reminiscent of those in the DKA model. At lower densities a front develops, which after some time settles into two full consecutive rows. At that point, these two rows cannot move, and thus the system becomes jammed after all the remaining particles drop onto these rows. The two consecutive rows always form in the direction normal to the driving. A snapshot of a 100×100 system in the DBKA model at $\rho = 0.6$ before the onset of jamming is shown in Fig. 9. The spontaneous formation of these jammed structures is the cause for the slow relaxation in the DBKA model, since it generally takes a very long time for this event to occur. Since the jammed structure in the DBKA model is one-dimensional, while in the other models it is two-dimensional, it requires much less time to form. Moreover, as the system size increases, the time for it to form, and therefore also the time for the system to reach the absorbing state, increases with the linear dimension L of the system, and not with the system size itself L^2. Hence, it is possible that in the infinite-size limit the formation of increasingly larger walls slows down the dynamics without letting the system ever reach the absorbing steady state.

In the BKA model at low densities two consecutive full rows or columns can be generated dynamically, which then behave as an unmovable wall inside the system. This wall can grow thicker as other particles form full rows or columns adjacent to it. However, outside the wall, the remaining particles are still active. These walls spontaneously form in either of the two axes. As the density increases the system becomes divided into rectangles with rattlers, which may be thought of as enclosures between two orthogonal pairs of parallel walls. If there are enough rattlers inside a rectangle, they can decrease the size of the rectangle by forming a full row or column adjacent to the rectangle's edge. If there are not enough rattlers to form a full row or column, they will continue rattling inside the rectangle forever. We hypothesize that in the infinite-size limit, the density of indefinitely rattling particles goes to zero.

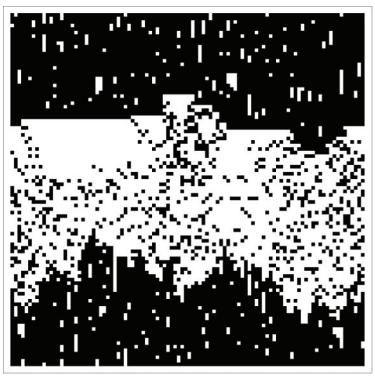

FIG. 9. A snapshot of a 100×100 system obtained from numerical simulation of the DBKA model at $\rho = 0.6$.

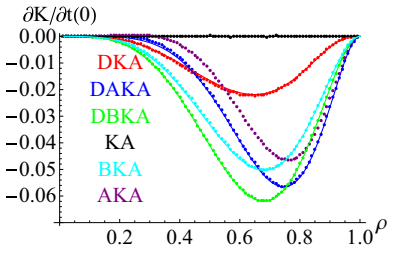

FIG. 10. The rate of change of the activity, $\partial K/\partial t$ at $t = 0$ from the simulations (symbols) and the SMF approximation (continuous lines). The numerical results are averages over 10^5 runs of 100×100 systems.

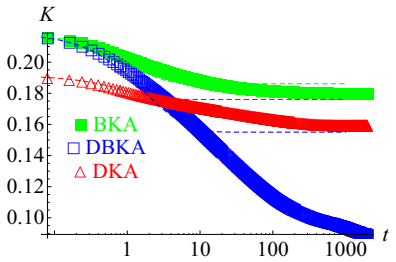

FIG. 11. The temporal behavior of the activity in the BKA, DBKA and DKA models for density $\rho = 0.5$. The dashed lines are the SMF approximation. The symbols are numerical results averaged over 10^5 runs of 100×100 systems.

The slow relaxation in the BKA model is due to the rare events of rattlers forming a full row or column and decreasing the size of the rectangle. Since the formation of the wall is a collective effect of $O(L)$ particles, the relaxation timescale increases with system size.

D. Temporal behavior of the activity

The SMF approximation can also be used to describe the temporal behavior of the activity. Starting from a random, uncorrelated initial condition, the SMF approximation can give insight into the short time dynamics, namely the temporal derivative of the activity at time $t = 0$, before correlations start developing in the system. Since at $t = 0$ the sites are uncorrelated, the exact activity at time $t = 0$ is equal to the MF prediction.

Since correlations haven't developed yet, the temporal derivative of the activity at time $t = 0$, $\partial K/\partial t|_{t=0}$, is exactly equal to that given by the SMF approximation with the probabilities P_α given by their MF values. Using Eq. (4), we find that for the driven models

$$\begin{aligned}
\left.\frac{\partial K^{\mathrm{DKA}}}{\partial t}\right|_{t=0} &= -\rho^4(1-\rho)^3(1+2\rho-\rho^3+2\rho^4 \\
&\quad +3\rho^5+\rho^6+\rho^7), \\
\left.\frac{\partial K^{\mathrm{DAKA}}}{\partial t}\right|_{t=0} &= -\rho^5(1-\rho)^2(1+3\rho+\rho^2), \\
\left.\frac{\partial K^{\mathrm{DBKA}}}{\partial t}\right|_{t=0} &= -\rho^4(1-\rho)^2(2+\rho+\rho^2-\rho^3). \qquad (8)
\end{aligned}$$

For the BKA model we find that

$$\left.\frac{\partial K^{\mathrm{BKA}}}{\partial t}\right|_{t=0} = -\frac{1}{4}\rho^4(1-\rho^2)^2(7+\rho+6\rho^2-4\rho^3). \qquad (9)$$

In these four models, $\partial K/\partial t$ at $t = 0$ is negative for all densities. Figure 10 shows the excellent agreement between the simulations and the analytically exact results. In the KA model, $\partial K^{\mathrm{KA}}/\partial t = 0$ at all times and for all densities, since correlations never develop there.

Numerically, we see in Fig. 11 that in the DKA, BKA and DBKA models, the activity decreases monotonically with time, while in Fig. 12 we see that in the AKA and DAKA models, the activity is not monotonic with time for $\rho < \rho_{\mathrm{m}}$, with $\rho_{\mathrm{m}}^{\mathrm{AKA}} \approx 0.66$ and $\rho_{\mathrm{m}}^{\mathrm{DAKA}} \approx 0.64$. As shown in Fig. 12, for $\rho < \rho_{\mathrm{m}}$ the activity in the AKA and DAKA models first decreases until it reaches a minimum at time t_{min}, then increases until it reaches the steady state, while for $\rho > \rho_{\mathrm{m}}$ it is monotonically decreasing. This result is counterintuitive; one would expect that the activity would either increase or decrease monotonically with time, depending on whether the system becomes less or more restricted.

The SMF approximation can qualitatively explain this behavior. Consider the evolution equation for P_{B} in the three driven models, given explicitly by

$$\begin{aligned}
\frac{\partial P_{\mathrm{B}}^{\mathrm{DKA}}}{\partial t} &= \frac{1-\rho^2}{1-\rho^3}\left(\rho - P_{\mathrm{B}}^{\mathrm{DKA}}\right)P_{\mathrm{F}}^{\mathrm{DKA}}, \\
\frac{\partial P_{\mathrm{B}}^{\mathrm{DAKA}}}{\partial t} &= \left[\frac{\rho(1-\rho^2)}{1-\rho^3} - P_{\mathrm{B}}^{\mathrm{DAKA}}\right]P_{\mathrm{F}}^{\mathrm{DAKA}}, \\
\frac{\partial P_{\mathrm{B}}^{\mathrm{DBKA}}}{\partial t} &= \left[\rho - P_{\mathrm{B}}^{\mathrm{DBKA}}\frac{1-\rho^2}{1-\rho^3}\right]P_{\mathrm{F}}^{\mathrm{DBKA}}, \qquad (10)
\end{aligned}$$

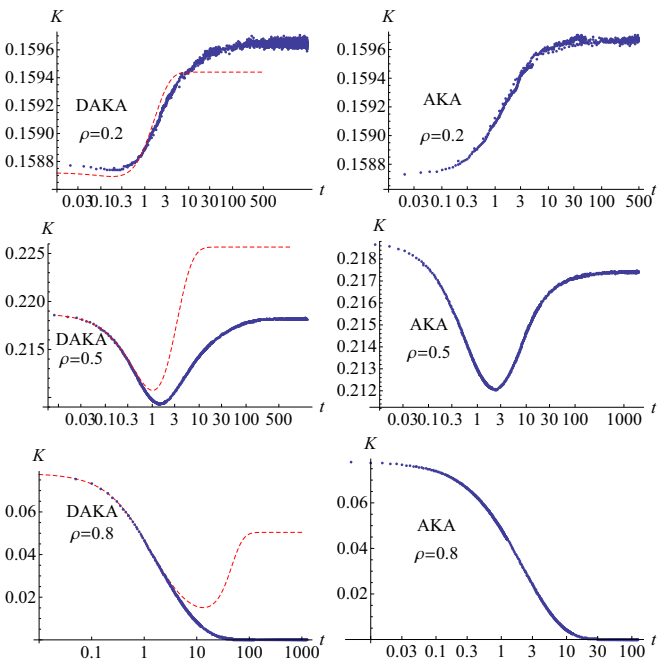

FIG. 12. The temporal behavior of the activity in the AKA and DAKA models for three different densities. The dotted red line is the SMF approximation. The blue dots are numerical results averaged over 10^5 runs of 100×100 systems.

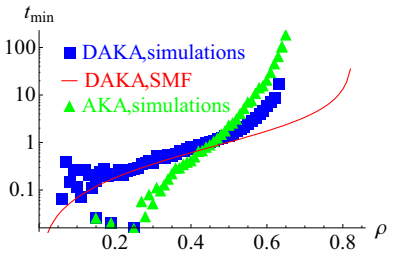

FIG. 13. The time at which the activity reaches a minimum, $t_{\min}$, as a function of density ρ, for numerical simulations (symbols) and the SMF approximation (solid line).

with the initial condition $P_B|_{t=0} = \rho$. In the DKA model, $P_B^{DKA} = \rho$ at all times, while in the DAKA (DBKA) model $\frac{\partial P_B}{\partial t}$ is negative (positive) for all ρ. This means that P_B^{DAKA} (P_B^{DBKA}) decreases (increases) monotonically with time from its initial value, ρ, to its steady-state value.

Now consider the evolution equation for P_F in the three driven models, which has the form

$$\frac{\partial P_F}{\partial t} = (C_0 + C_B P_B + C_F P_F) P_F, \tag{11}$$

where C_0, C_B, and C_F depend only on the density. For the DKA and DBKA models, $\partial P_F/\partial t$ is negative for all values of P_B and P_F between their initial values and the steady-state values, for all densities, and thus P_F in these two models monotonically decreases with time, and so does the activity. In the DAKA model, however, there are values of P_B and P_F between their initial and steady-state values for which $\partial P_F/\partial t$ is positive. Furthermore, for P_B^{DAKA} equal to its steady-state value, and $\rho < \rho_{DAKA}^{SMF} \approx 0.933$, we find that $\partial P_F/\partial t$ is positive for all values of P_F^{DAKA} between its initial and steady-state values.

Figure 13 shows the value of $t_{\min}$ versus the density. The SMF approximation predicts that $t_{\min}$ diverges at $\rho_m^{DAKA} \approx 0.827$, while according to the simulations it diverges at $\rho \approx 0.64$.

IV. DISCUSSION

In this paper we showed that counterintuitively, adding transitions to a dynamical system that increase its activity in the MF approximation may in fact decrease its activity. We analyzed this scenario by investigating six related lattice gas models: the equilibrium KA model, and five nonequilibrium variants of it (AKA, BKA, DKA, DAKA, DBKA). In some cases adding such transitions increases the activity (DKA $\rightarrow$ DAKA, KA $\rightarrow$ AKA at small densities) as intuitively expected, while in other cases it surprisingly decreases the activity (DKA $\rightarrow$ DBKA, KA $\rightarrow$ BKA).

The difference lies in the topology of the phase space for each model. For example, consider the undriven models KA, AKA, and BKA. The phase space of the KA model is composed of a large part which contains states in which none of the particles are permanently frozen, and many small parts each of them contains states in which a specific subset of the particles cannot move, most of them due to the particles being in two (or more) consecutive rows or columns. The AKA and BKA models add transitions between the different disjoined parts. In the BKA model, the permanently frozen walls cannot be broken, but they can form dynamically. Therefore, the added transitions in the BKA model between the different parts of the state space is into a more jammed structure. In the AKA model, the permanently frozen walls can be broken, and so the added transitions between the parts allow the system to escape from these jammed parts. At high enough density, there are other jammed structures which are 2D in nature, not quasi-1D as the walls. The AKA model also allows transitions into these 2D jammed structures, but not out of them, and thus at high enough density it also jams.

The appearance of these jammed structures is the precursor to the system reaching an absorbing state, in which none of the particles can move. In an infinite system, qualitatively described by our SMF approximation, the time to reach an absorbing state is either finite above the critical density and then the steady-state activity is zero, or infinite below it and then the steady-state activity is finite. In a finite-size system below the critical density, the system will eventually reach the absorbing state, however before that it reaches a long-lived metastable state with a finite activity, the life time of which increases exponentially with the system size.

It would be interesting to continue investigating the models we described in this paper: AKA, DAKA, BKA, and DBKA. For example, the critical density we found in the simulations is for a system of size 30×30, and there are bound to be finite-size effects. As these models exhibit an absorbing state phase transition, a natural question is what universality class do they belong to. We conjecture that the DKA, AKA, and DAKA models all belong to the same class, while the BKA and DBKA belong to a different class. Also, our simulations started from an uncorrelated initial condition, and an interesting question is how does the initial condition affects the dynamics, since the initial conditions affect even models which obey detailed balance [56]. Other points which are worth investigating are the correlations and the relaxation time, especially in the BKA and DBKA models.

ACKNOWLEDGMENTS

We thank Gregory Bolshak, Rakesh Chatterjee, Paul Krapivsky, Carl Merrigan, and Erdal Oğuz for fruitful discussions. This research was supported in part by the Israel Science Foundation Grant No. 968/16 and by the National Science Foundation Grant No. NSF PHY-1748958.

APPENDIX A: DERIVATION OF THE TRANSITION RATES IN THE DRIVEN MODELS

In this Appendix we derive the transition rates for the three driven models. Each possible transition is illustrated in the configuration before the move, and an arrow shows which particle moves where. The particle whose state changes between free, blocked, and jammed is called the *main particle*, and it is marked in the illustrations with a green circle. A site with an empty circle represent an occupied site, and a site without any mark represent a vacant site. Other symbols represent sites which may or may not be occupied and are specified for each rate. In the derivation of the rates, we use various kinds of conditional probabilities, which are evaluated in Sec. A 1.

TABLE I. The rates $\omega_{\alpha,\beta}$ and $\Omega_{\alpha,\beta}$ for the three driven models.

	DKA	DAKA	DBKA
$\omega_{\mathrm{B,J}}$	$\frac{\rho^3(1-\rho^2)}{1-\rho^3}$	ρ^2	$\frac{\rho^3(1-\rho^2)}{1-\rho^3}$
$\omega_{\mathrm{B,F}}$	$1-\rho^2$	$1-\rho^2$	$1-\rho^2$
$\omega_{\mathrm{J,F}}$	$\frac{1}{2-\rho^3}[1+\frac{2(1-\rho^2)}{1-\rho^3}+\frac{2(1-\rho^2)^2}{(1-\rho^3)^2}]$	$1+2\frac{1-\rho^2}{1-\rho^3}$	$2\frac{1-\rho^2}{1-\rho^3}$
$\Omega_{\mathrm{F,B}}$	$\frac{\rho(1-\rho^2)}{1-\rho^3}$	$\frac{\rho(1-\rho^2)}{1-\rho^3}$	ρ
$\omega_{\mathrm{F,J}}$	$\frac{\rho^3(1-\rho^2)}{(1-\rho^3)^2}[1+\frac{2(1-\rho)(2+2\rho-\rho^3)}{(1-\rho^3)^2}]$	$\frac{2\rho^3}{(1-\rho^3)^2}$	$\frac{\rho^3}{1-\rho^3}(1+2\frac{1-\rho^2}{1-\rho^3})$
$\Omega_{\mathrm{F,J}}$	$\frac{\rho^3(1-\rho)}{1-\rho^3}$	$\frac{\rho^3(1-\rho)}{1-\rho^3}$	0

The rates for the DAKA, DBKA and DKA model are derived in Secs. A 2, A 3, and A 4, respectively. The derived rates $\omega_{\alpha,\beta}$ and $\Omega_{\alpha,\beta}$ for the three driven models, related to the rates $r_{\alpha,\beta}$ via Eq. (6), are summarized in Table I. Note that $\omega_{\mathrm{J,B}} = \omega_{\mathrm{F,B}} = 0$ for all the driven models, since a particle can change into a blocked state only if it moves downwards.

1. Conditional probabilities

In this section we evaluate several conditional probabilities by using a MF approach. We start with the probability that a particle is free given that one of its constraining sites is occupied, $P_{\mathrm{F}|\rho}$. The conditional probability is given by

$$P_{\mathrm{F}|\rho} = \frac{P_{\mathrm{F}\cap\rho}}{\rho}, \tag{A1}$$

where $P_{\mathrm{F}\cap\rho}$ is the probability that the particle is free *and* one of its constraining sites is occupied. We approximate $P_{\mathrm{F}\cap\rho}$ as P_{F} multiplied by the mean-field fraction of free configurations with one constraining site occupied,

$$P_{\mathrm{F}\cap\rho} = \frac{\rho(1-\rho^2)}{1-\rho^3}P_{\mathrm{F}}. \tag{A2}$$

Hence,

$$P_{\mathrm{F}|\rho} = \frac{(1-\rho^2)}{1-\rho^3}P_{\mathrm{F}}. \tag{A3}$$

In a similar fashion, we find that the probability that a particle is free given that one of its constraining sites is vacant, $P_{\mathrm{F}|\mathrm{v}}$, is

$$P_{\mathrm{F}|\mathrm{v}} = \frac{P_{\mathrm{F}\cap\mathrm{v}}}{1-\rho} = \frac{1}{1-\rho^3}P_{\mathrm{F}}. \tag{A4}$$

The probability that a particle is free given that the site below is vacant, $P_{\mathrm{F}|\mathrm{t}}$, is

$$P_{\mathrm{F}|\mathrm{t}} = \frac{P_{\mathrm{F}\cap\mathrm{t}}}{1-\rho} = \frac{P_{\mathrm{F}}}{1-\rho}. \tag{A5}$$

the probability that a particle is free given that one of its constraining sites is occupied and the site below it is vacant, $P_{\mathrm{F}|\rho\mathrm{t}}$, is

$$P_{\mathrm{F}|\rho\mathrm{t}} = \frac{P_{\mathrm{F}\cap\rho\cap\mathrm{t}}}{\rho(1-\rho)} = \frac{P_{\mathrm{F}\cap\rho}}{\rho(1-\rho)} = \frac{P_{\mathrm{F}|\rho}}{1-\rho}. \tag{A6}$$

The probability that a particle is free given that one of its constraining sites and the site below it are vacant, $P_{\mathrm{F}|\mathrm{vt}}$, is

$$P_{\mathrm{F}|\mathrm{vt}} = \frac{P_{\mathrm{F}\cap\mathrm{v}\cap\mathrm{t}}}{(1-\rho)^2} = \frac{P_{\mathrm{F}\cap\mathrm{v}}}{(1-\rho)^2} = \frac{P_{\mathrm{F}|\mathrm{v}}}{1-\rho}. \tag{A7}$$

The probability that a site is occupied given that it is a constraining site of a free particle, $P_{\rho|\mathrm{F}}$, is given by

$$P_{\rho|\mathrm{F}} = \frac{P_{\mathrm{F}\cap\rho}}{P_{\mathrm{F}}} = \frac{\rho(1-\rho^2)}{1-\rho^3}, \tag{A8}$$

and the probability that a site is vacant given that it is a constraining site of a free particle, $P_{v|\mathrm{F}}$, is given by

$$P_{v|\mathrm{F}} = \frac{P_{\mathrm{F}\cap\mathrm{v}}}{P_{\mathrm{F}}} = \frac{1-\rho}{1-\rho^3}, \tag{A9}$$

The probability that two sites are occupied given that they are constraining sites in the same group of a free particle, $P_{\rho^2|\mathrm{F}}$, is given by

$$P_{\rho^2|\mathrm{F}} = \frac{P_{\mathrm{F}\cap\rho^2}}{P_{\mathrm{F}}} = \frac{\rho^2(1-\rho)}{1-\rho^3}. \tag{A10}$$

In the DKA model, we are also interested in the probabilities that a particle is free given some condition on both groups of constraining particles, $P_{\mathrm{F}|s_1,s_2}$, and the probabilities that the two groups satisfy a certain condition given that they are constraining groups of a free particle, $P_{s_1,s_2|\mathrm{F}}$. Since in the MF approximation the occupancies of the two groups are independent of each other, we find that

$$P_{\mathrm{F}|s_1,s_2} = \frac{P_{\mathrm{F}|s_1}P_{\mathrm{F}|s_2}}{P_{\mathrm{F}}},$$
$$P_{s_1,s_2|\mathrm{F}} = P_{s_1|\mathrm{F}}P_{s_2|\mathrm{F}}. \tag{A11}$$

Similarly, the probability that a particle is free given some conditions on both groups of constraining particles and that the site below is vacant, $P_{\mathrm{F}|s_1,s_2,\mathrm{t}}$, is given by

$$P_{\mathrm{F}|s_1,s_2,\mathrm{t}} = \frac{P_{\mathrm{F}|s_1,s_2}}{1-\rho}. \tag{A12}$$

We are also interested in the conditional probabilities in the DKA model that the two constraining groups are in a certain configuration given that the main particle is jammed. Specifically, the probability that one of the constraining groups is fully occupied and the other is not, $P_{\rho^3,1-\rho^3|\mathrm{J}}$, and the probability that one of the constraining groups is fully occupied and in the other one specific site is vacant and at least one of the other two is also vacant, $P_{\rho^3,v(1-\rho^2)}$. These probabilities are given by

$$P_{\rho^3,1-\rho^3|\mathrm{J}} = \frac{P_{\mathrm{J}\cap\rho^3\cap1-\rho^3}}{P_{\mathrm{J}}} = \frac{\rho^3(1-\rho^3)}{\rho^6+2\rho^3(1-\rho^3)},$$
$$P_{\rho^3,v(1-\rho^2)|\mathrm{J}} = \frac{P_{\mathrm{J}\cap\rho^3\cap\mathrm{v}(1-\rho^2)}}{P_{\mathrm{J}}} = \frac{\rho^3(1-\rho)(1-\rho^2)}{\rho^6+2\rho^3(1-\rho^3)}. \tag{A13}$$

2. DAKA model

a. $r_{\mathrm{B,J}}^{\mathrm{DAKA}}$ *and* $r_{\mathrm{B,F}}^{\mathrm{DAKA}}$

Before the move, the blocked configuration consists of the main particle (green circle in Fig. 14) and the blocking particle (empty circle). The state of the main particle can change only if the blocked particle moves. The blocked particle can move with probability $P_{\mathrm{F}}^{\mathrm{DAKA}}$, since the occupancy of the three sites comprising its kinetic constraint (purple $\times$) is irrelevant to the state of the main particle either before or after the move. If both sites marked with a blue $\diamond$ are occupied, which occurs

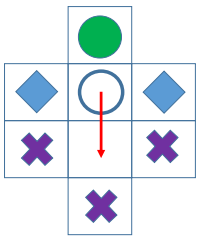

FIG. 14. An illustration of the transitions B → J and B → F in the DAKA model.

with probability ρ^2, then after the move the main particle will be jammed, otherwise it will be free. Therefore,

$$r_{\mathrm{B,J}}^{\mathrm{DAKA}} = \rho^2 P_{\mathrm{F}},$$
$$r_{\mathrm{B,F}}^{\mathrm{DAKA}} = (1-\rho^2)P_{\mathrm{F}}. \tag{A14}$$

b. $r_{\mathrm{J,F}}^{\mathrm{DAKA}}$ *and* $r_{\mathrm{J,B}}^{\mathrm{DAKA}}$

Before the move, the jammed configuration consists of the main particle (green circle in Fig. 15) and the three jamming particles (empty circles). The state of the main particle can change only if one of the three jamming particles moves, and it can only change to a free state, not a blocked state, hence

$$r_{\mathrm{J,B}}^{\mathrm{DAKA}} = 0. \tag{A15}$$

The middle jamming particle [Fig. 15(a)] can move with probability P_{F}, while the jamming particles on the two sides [Fig. 15(b)] can move with probability $P_{\mathrm{F}|\rho}$. Therefore, the rate $r_{\mathrm{J,F}}^{\mathrm{DAKA}}$ is

$$r_{\mathrm{J,F}}^{\mathrm{DAKA}} = P_{\mathrm{F}} + 2P_{\mathrm{F}|\rho} = P_{\mathrm{F}} + 2\frac{1-\rho^2}{1-\rho^3}P_{\mathrm{F}}. \tag{A16}$$

c. $r_{\mathrm{F,B}}^{\mathrm{DAKA}}$

Before the move the configuration consists of the main free particle (green circle in Fig. 16) and the particle which will block the main particle after the move (empty circle). The rate is given by the probability that the bottom site is occupied given that the main particle is free, $P_{\rho|\mathrm{F}}$, and thus

$$r_{\mathrm{F,B}}^{\mathrm{DAKA}} = P_{\rho|\mathrm{F}} = \frac{\rho(1-\rho^2)}{1-\rho^3}. \tag{A17}$$

d. $r_{\mathrm{F,J}}^{\mathrm{DAKA}}$

There are two ways in which a free particle can change into a jammed particle. In the first case, illustrated in Fig. 17(a),

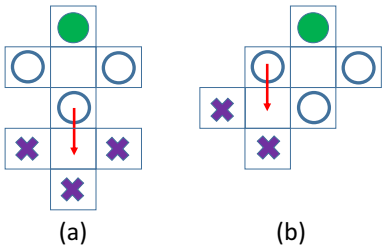

FIG. 15. An illustration of the transition J → F in the DAKA model.

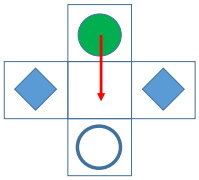

FIG. 16. An illustration of the transition F → B in the DAKA model.

the main particle moves into a jammed configuration. This happens if the three jamming sites are occupied, which occur with probability ρ^3, and if the site between them is vacant, which occur with probability $P_{v|\mathrm{F}}$. Therefore, the rate for the first case is

$$r_{\mathrm{F,J}}^{DAKA,1} = \rho^3 P_{v|\mathrm{F}} = \frac{\rho^3(1-\rho)}{1-\rho^3}. \tag{A18}$$

In the second case, illustrated in Fig. 17(b), a particle moves to occupy one of neighbors of the main particle. The rate for this case is

$$r_{\mathrm{F,J}}^{DAKA,2} = 2P_{\rho^2|\mathrm{F}}\rho P_{\mathrm{F}|\mathrm{vt}} = \frac{2\rho^3}{(1-\rho^3)^2}P_{\mathrm{F}}. \tag{A19}$$

The total rate $r_{\mathrm{F,J}}^{\mathrm{DAKA}}$ is given by

$$r_{\mathrm{F,J}}^{\mathrm{DAKA}} = r_{\mathrm{F,J}}^{DAKA,1} + r_{\mathrm{F,J}}^{DAKA,2}. \tag{A20}$$

3. DBKA model

a. $r_{\mathrm{B,J}}^{\mathrm{DBKA}}$ *and* $r_{\mathrm{B,F}}^{\mathrm{DBKA}}$

The main particle (green circle in Fig. 18) can change its state only if the blocking particle (empty circle) moves. The rates are therefore

$$r_{\mathrm{B,J}}^{\mathrm{DBKA}} = \rho^3 P_{\mathrm{F}|\rho} = \frac{\rho^3(1-\rho^2)}{1-\rho^3}P_{\mathrm{F}},$$
$$r_{\mathrm{B,F}}^{\mathrm{DBKA}} = (1-\rho^3)P_{\mathrm{F}|\rho} = (1-\rho^2)P_{\mathrm{F}}. \tag{A21}$$

b. $r_{\mathrm{J,B}}^{\mathrm{DBKA}}$ *and* $r_{\mathrm{J,F}}^{\mathrm{DBKA}}$

The main jammed particle (green circle in Fig. 19) can change its state only if one of its two side neighbors move. The rates are therefore

$$r_{\mathrm{J,B}}^{\mathrm{DBKA}} = 0,$$
$$r_{\mathrm{J,F}}^{\mathrm{DBKA}} = 2P_{\mathrm{F}|\rho} = 2\frac{1-\rho^2}{1-\rho^3}P_{\mathrm{F}}. \tag{A22}$$

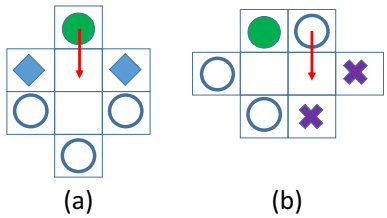

FIG. 17. An illustration of the transition F → J in the DAKA model.

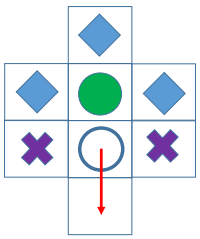

FIG. 18. An illustration of the transitions B → J and B → F in the DBKA model.

c. $r_{\mathrm{F,B}}^{\mathrm{DBKA}}$ *and* $r_{\mathrm{F,J}}^{\mathrm{DBKA}}$

The transition F → B is illustrated in Fig. 20(a), and its rate is

$$r_{\mathrm{F,B}}^{\mathrm{DBKA}} = \rho. \tag{A23}$$

The transition F → J can occur in two different ways illustrated in Figs. 20(b) and 20(c). The corresponding rates for the two cases are

$$\begin{aligned} r_{\mathrm{F,J}}^{DBKA,1} &= P_{\rho^2|\mathrm{F}}\rho P_{\mathrm{F}|\mathrm{t}} = \frac{\rho^3}{1-\rho^3}P_{\mathrm{F}}, \\ r_{\mathrm{F,J}}^{DBKA,2} &= 2P_{\rho^2|\mathrm{F}}\rho P_{\mathrm{F}|\rho\mathrm{t}} = \frac{2\rho^3(1-\rho^2)}{(1-\rho^3)^2}P_{\mathrm{F}}. \end{aligned} \tag{A24}$$

The total rate is therefore

$$r_{\mathrm{F,J}}^{\mathrm{DBKA}} = r_{\mathrm{F,J}}^{DBKA,1} + r_{\mathrm{F,J}}^{DBKA,2} = \frac{\rho^3}{1-\rho^3}\left(1+2\frac{1-\rho^2}{1-\rho^3}\right)P_{\mathrm{F}}. \tag{A25}$$

4. DKA model

a. $r_{\mathrm{B,J}}^{\mathrm{DKA}}$ *and* $r_{\mathrm{B,F}}^{\mathrm{DKA}}$

Similarly to the corresponding rates in the DAKA and DBKA model, these transitions occur only when the blocking particle (empty circle in Fig. 21) moves. In order for it to be free, it requires that at least one of its three neighbors after the move (purple ×) is vacant, and that at least one of its three neighbors before the move (the main particle depicted as a green circle and the two yellow stars) is vacant. Since the main particle already occupies one site, this transition is possible only if at least one of the two sites marked with a yellow star is vacant, which itself means that in order for the main particle to be jammed after the blocking particle moves, all three sites marked with a ⋄ must be occupied, otherwise it will be free after the blocking particle moves. Therefore, the

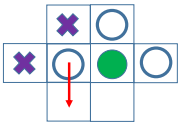

FIG. 19. An illustration of the transition J → F in the DBKA model.

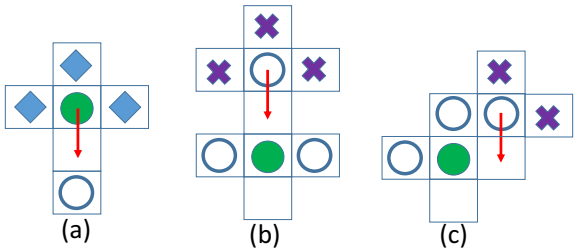

FIG. 20. An illustration of the transitions F → B and F → J in the DBKA model.

rates are

$$\begin{aligned} r_{\mathrm{B,J}}^{\mathrm{DKA}} &= \rho^3 P_{\mathrm{F}|\rho} = \frac{\rho^3(1-\rho^2)}{1-\rho^3}P_{\mathrm{F}}, \\ r_{\mathrm{B,F}}^{\mathrm{DKA}} &= (1-\rho^3)P_{\mathrm{F}|\rho} = (1-\rho^2)P_{\mathrm{F}}. \end{aligned} \tag{A26}$$

b. $r_{\mathrm{J,B}}^{\mathrm{DKA}}$ *and* $r_{\mathrm{J,F}}^{\mathrm{DKA}}$

A jammed particle can change its state only if one of its neighbors moves, which causes it to become free. Therefore,

$$r_{\mathrm{J,B}}^{\mathrm{DKA}} = 0. \tag{A27}$$

The transition J → F may occur in three different ways, illustrated in Fig. 22. In the first case, shown in Fig. 22(a), at least one of the three sites marked ⋄ is vacant, and at least one of the sites marked × is vacant. The corresponding rate is

$$r_{\mathrm{J,F}}^{DKA,1} = P_{\rho^3(1-\rho^3)|\mathrm{J}}P_{\mathrm{F}|\mathrm{v}} = \frac{1}{2-\rho^3}P_{\mathrm{F}}. \tag{A28}$$

In the second case, shown in Fig. 22(b), at least one of the three sites marked ⋄ is vacant, and at least one of the two sites marked × is vacant. The corresponding rate is

$$r_{\mathrm{J,F}}^{DKA,2} = 2P_{\rho^3(1-\rho^3)|\mathrm{J}}P_{\mathrm{F}|\mathrm{v},\rho} = 2\frac{1-\rho^2}{(2-\rho^3)(1-\rho^3)}P_{\mathrm{F}}. \tag{A29}$$

In the third case, shown in Fig. 22(c), at least one of the two sites marked ⋄ is vacant, and at least one of the two sites marked × is vacant. The corresponding rate is

$$r_{\mathrm{J,F}}^{DKA,3} = 2P_{\rho^3 v(1-\rho^2)|\mathrm{J}}P_{\mathrm{F}|\rho,\mathrm{v},\mathrm{t}} = 2\frac{(1-\rho^2)^2}{(2-\rho^3)(1-\rho^3)^2}P_{\mathrm{F}}. \tag{A30}$$

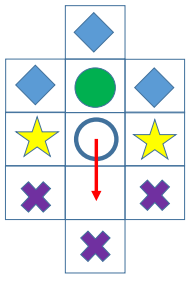

FIG. 21. An illustration of the transitions B → J and B → F in the DKA model.

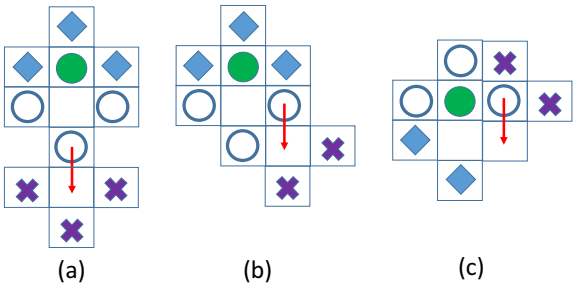

FIG. 22. An illustration of the transitions J → F in the DKA model.

c. $r_{F,B}^{DKA}$

This transition is shown in Fig. 23, and the rate is

$$r_{F,B}^{DKA} = P_{\rho|F} = \frac{\rho(1-\rho^2)}{1-\rho^3}. \tag{A31}$$

d. $r_{F,J}^{DKA}$

There are five ways to transition from a free state to a jammed state. In the first case, shown in Fig. 24(a), at least one of the three ⋄ sites is vacant, at least one of the three × sites is vacant, and at least one of the two ∗ sites is vacant. The corresponding rate is

$$r_{F,J}^{DKA,1} = \rho P_{\rho^2|F} P_{F|\rho,t} = \frac{\rho^3(1-\rho^2)}{(1-\rho^3)^2} P_F. \tag{A32}$$

In the second case, shown in Fig. 24(b), at least one of the two × sites is vacant, and the corresponding rate is

$$r_{F,J}^{DKA,2} = 2\rho P_{\rho^2,v|F} P_{F|\rho,v\rho,t} = 2\frac{\rho^3(1-\rho)(1-\rho^2)}{(1-\rho^3)^4} P_F. \tag{A33}$$

In the third case, shown in Fig. 24(c), at least one of the two ⋄ sites is vacant and at least one of the two × sites is vacant. The corresponding rate is

$$r_{F,J}^{DKA,3} = 2\rho v P_{\rho^2,\rho|F} P_{F|\rho,\rho^2 v,t} = 2\frac{\rho^4(1-\rho)(1-\rho^2)^2}{(1-\rho^3)^4} P_F. \tag{A34}$$

In the fourth case, shown in Fig. 24(d), at least one of the two ⋄ sites and at least one of the two × sites are vacant. The corresponding rate is

$$r_{F,J}^{DKA,4} = 2P_{\rho,\rho^2 v|F} P_{F|\rho,v,t} = 2\frac{\rho^3(1-\rho^2)^2}{(1-\rho^3)^4} P_F. \tag{A35}$$

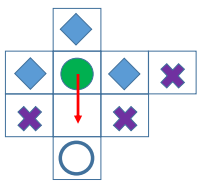

FIG. 23. An illustration of the transition F → B in the DKA model.

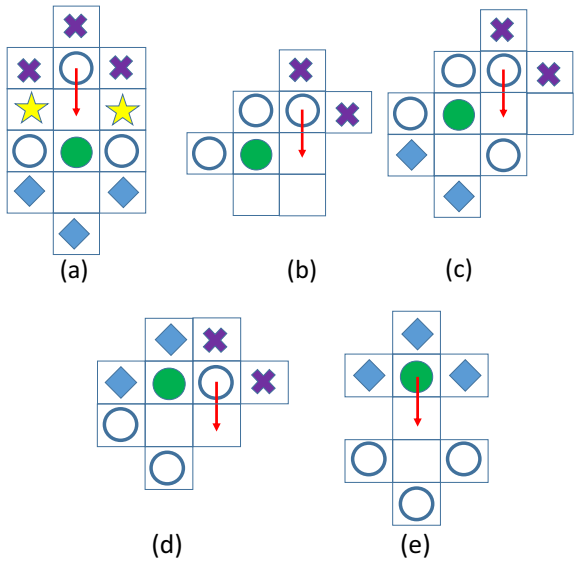

FIG. 24. An illustration of the transition F → J in the DKA model.

In the fifth case, shown in Fig. 24(e), at least one of the three ⋄ sites is vacant and the corresponding rate is

$$r_{F,J}^{DKA,5} = \rho^3 P_{v|F} = \frac{\rho^3(1-\rho)}{1-\rho^3}. \tag{A36}$$

APPENDIX B: STABILITY OF THE STATIONARY SOLUTION

In this Appendix we show that whenever the nontrivial stationary solution exists, it is also stable. Using Eq. (3), the evolution equations for P_B and P_F are explicitly

$$\begin{aligned}\frac{\partial P_B}{\partial t} &= [\Omega_{F,B} + \omega_{F,B}P_F + \omega_{J,B}(1-P_B-P_F) \\ &\quad - (\omega_{B,J}+\omega_{B,F})P_B]P_F, \\ \frac{\partial P_F}{\partial t} &= [\omega_{B,F}P_B + \omega_{J,F}(1-P_B-P_F) \\ &\quad - (\Omega_{F,B} + \omega_{F,B}P_F + \Omega_{F,J} + \omega_{F,J}P_F)]P_F,\end{aligned} \tag{B1}$$

which can be written in matrix form as

$$\frac{\partial}{\partial t}\begin{pmatrix}P_B\\P_F\end{pmatrix} = P_F\left[\mathcal{M}\begin{pmatrix}P_B\\P_F\end{pmatrix} + \begin{pmatrix}P_B^0\\P_F^0\end{pmatrix}\right], \tag{B2}$$

with the matrix $\mathcal{M}$ given explicitly by

$$\mathcal{M} = -\begin{pmatrix}\omega_{J,B}+\omega_{B,J}+\omega_{B,F} & \omega_{J,B}-\omega_{F,B}\\ \omega_{J,F}-\omega_{B,F} & \omega_{J,F}+\omega_{F,B}+\omega_{F,J}\end{pmatrix}, \tag{B3}$$

and the vector $\begin{pmatrix}P_B^0\\P_F^0\end{pmatrix}$ by

$$\begin{pmatrix}P_B^0\\P_F^0\end{pmatrix} = \begin{pmatrix}\Omega_{F,B}+\omega_{J,B}\\ \omega_{J,F}-\Omega_{F,B}-\Omega_{F,J}\end{pmatrix}. \tag{B4}$$

The determinant of $\mathcal{M}$ is

$$\begin{aligned}|\mathcal{M}| &= (\omega_{F,B}+\omega_{F,J})(\omega_{B,J}+\omega_{J,B}) \\ &\quad + (\omega_{B,J}+\omega_{F,B})\omega_{J,F} + \omega_{B,F}(\omega_{F,J}+\omega_{J,B}+\omega_{J,F}),\end{aligned} \tag{B5}$$

which is positive since for any set of kinetic constraints, including for models we do not consider here, $\omega_{\mathrm{J,F}}$ and at least one of $\omega_{\mathrm{B,F}}$ and $\omega_{\mathrm{B,J}}$ are positive.

We now look for stationary solutions of Eq. (4) under the condition $0 \leqslant P_{\mathrm{F}}, P_{\mathrm{J}}, P_{\mathrm{B}} \leqslant 1$. The solution $P_{\mathrm{F}} = 0$ is always a stationary solution. We find that if there is another stationary solution with $P_{\mathrm{F}} > 0$, then it is unique and given by

$$\begin{pmatrix} P_{\mathrm{B}} \\ P_{\mathrm{F}} \end{pmatrix}_{ss} = -\mathcal{M}^{-1} \begin{pmatrix} P_{\mathrm{B}}^0 \\ P_{\mathrm{F}}^0 \end{pmatrix}. \tag{B6}$$

In order to check its stability, we perturb P_{B} and P_{F} around it, such that $P_\alpha = P_{\alpha,ss} + \delta_\alpha$. Setting this perturbation in Eq. (B2) yields

$$\begin{aligned} \frac{\partial}{\partial t}\begin{pmatrix} \delta_{\mathrm{B}} \\ \delta_{\mathrm{F}} \end{pmatrix} &= (P_{\mathrm{F,ss}} + \delta_{\mathrm{F}}) \left[\mathcal{M} \begin{pmatrix} P_{\mathrm{B}} \\ P_{\mathrm{F}} \end{pmatrix} + \mathcal{M} \begin{pmatrix} \delta_{\mathrm{B}} \\ \delta_{\mathrm{F}} \end{pmatrix} + \begin{pmatrix} P_{\mathrm{B}}^0 \\ P_{\mathrm{F}}^0 \end{pmatrix} \right] \\ &= \delta_{\mathrm{F}} \left[\mathcal{M} \begin{pmatrix} P_{\mathrm{B}} \\ P_{\mathrm{F}} \end{pmatrix} + \begin{pmatrix} P_{\mathrm{B}}^0 \\ P_{\mathrm{F}}^0 \end{pmatrix} \right] + P_{\mathrm{F,ss}} \mathcal{M} \begin{pmatrix} \delta_{\mathrm{B}} \\ \delta_{\mathrm{F}} \end{pmatrix}, \end{aligned} \tag{B7}$$

where in the second step we kept terms linear in δ_α. Using Eq. (B6) yields

$$\frac{\partial}{\partial t}\begin{pmatrix} \delta_{\mathrm{B}} \\ \delta_{\mathrm{F}} \end{pmatrix} = P_{\mathrm{F,ss}} \mathcal{M} \begin{pmatrix} \delta_{\mathrm{B}} \\ \delta_{\mathrm{F}} \end{pmatrix}. \tag{B8}$$

Since $P_{\mathrm{F,ss}} > 0$, the steady-state solution is stable if the real part of both eigenvalues of $\mathcal{M}$ is negative. The two eigenvalues of $\mathcal{M}$ have the form

$$\lambda_\pm = -\lambda_0 \pm \lambda_1, \tag{B9}$$

where $\lambda_0 > 0$ and λ_1 can be negative, positive, or imaginary. Therefore, only λ_+ can have a positive real part, and that occurs only if λ_1 is positive. However, in that case $\lambda_- < 0$, and since $|\mathcal{M}| > 0$, and thus λ_+ must also be negative. Hence, if the nontrivial stationary solution exists, it is also stable.

APPENDIX C: STABILITY OF THE $P_{\mathrm{F}} = 0$ SOLUTION

In this Appendix we investigate the stability of the $P_{\mathrm{F}} = 0$ state in the SMF approximation. We start from the driven models, and then consider the BKA model.

1. Driven models

In order to check the stability of the $P_{\mathrm{F}} = 0$ state in the driven models, we perturb P_{B} and P_{F} around it, such that $P_{\mathrm{F}} = \delta_{\mathrm{F}}$ and $P_{\mathrm{B}} = P_{\mathrm{B,ss}} + \delta_{\mathrm{B}}$. Setting this perturbation in Eq. (B2) and keeping only terms linear in δ_{B} and δ_{F} yields

$$\frac{\partial}{\partial t}\begin{pmatrix} \delta_{\mathrm{B}} \\ \delta_{\mathrm{F}} \end{pmatrix} = \delta_{\mathrm{F}} \begin{pmatrix} \omega_{\mathrm{B}} \\ \omega_{\mathrm{F}} \end{pmatrix}, \tag{C1}$$

with

$$\begin{aligned} \omega_{\mathrm{B}} &= \Omega_{\mathrm{F,B}} + \omega_{\mathrm{J,B}} - (\omega_{\mathrm{J,B}} + \omega_{\mathrm{B,J}} + \omega_{\mathrm{B,F}}) P_{\mathrm{B,ss}}, \\ \omega_{\mathrm{F}} &= (\omega_{\mathrm{B,F}} - \omega_{\mathrm{J,F}}) P_{\mathrm{B,ss}} - (\Omega_{\mathrm{F,B}} + \Omega_{\mathrm{F,J}} - \omega_{\mathrm{J,F}}). \end{aligned} \tag{C2}$$

For any value of ρ we find a critical $P_{\mathrm{B,c}}$ above which $\omega_{\mathrm{F}} < 0$ and thus the $P_{\mathrm{F}} = 0$ solution is stable. This critical $P_{\mathrm{B,ss}}$ is

$$\begin{aligned} P_{\mathrm{B,c}}^{\mathrm{DAKA}} &= \frac{3 + 2\rho - \rho^3}{2 + 2\rho + \rho^2 + \rho^3 + \rho^4}, \quad P_{\mathrm{B,c}}^{\mathrm{DBKA}} = \frac{2 + \rho - \rho^2 - \rho^3}{(1+\rho)(1+\rho^3)}, \\ P_{\mathrm{B,c}}^{\mathrm{DKA}} &= \frac{5 + 8\rho + 5\rho^2 - 2\rho^3 - 2\rho^4 + 3\rho^6 + 2\rho^7 + \rho^8}{3 + 6\rho + 5\rho^2 + 5\rho^3 + 7\rho^4 + 6\rho^5 + 2\rho^6 - 2\rho^7 - 2\rho^8 - \rho^9}. \end{aligned} \tag{C3}$$

Note that $P_{\mathrm{B,c}} > 1$ for $\rho < 0.618$ for all three models, which means that the $P_{\mathrm{F}} = 0$ solution is unstable for $\rho < 0.618$. The value of 0.618 is the root of the polynomial $1 - \rho^2(1+\rho)^2$.

In the BKA model, there are six states as outlined in Appendix D. In two of them, B4 and B3J, the particle cannot move and in the other four the particle can move in at least one direction. The trivial stationary solution in this model is $P_{\mathrm{B3J}} = 1 - P_{\mathrm{B4}}$ and $P_{\mathrm{B2F2}} = P_{\mathrm{BFBF}} = P_{\mathrm{BF3}} = P_{\mathrm{F4}} = 0$. Perturbing the evolution equation around this solution to first order in the perturbation yields equations of the form

$$\frac{\partial \delta_\alpha}{\partial t} = \sum_\beta (\omega_{\beta,\alpha} + \Omega_{\beta,\alpha} P_{\mathrm{B}}) \delta_\beta, \tag{C4}$$

where $\omega_{\beta,\alpha}$ and $\Omega_{\beta,\alpha}$ depend only on the density, and α and β are the states in which the particle can move in at least one direction. This may be written in matrix form as

$$\frac{\partial}{\partial t}\delta = (\omega + P_{\mathrm{B}}\Omega)\delta. \tag{C5}$$

The trivial stationary solution is stable if the real part of all the four eigenvalues of the matrix $\omega + P_{\mathrm{B}}\Omega$ is negative. Investigating this matrix numerically we find that all its eigenvalues are real, and that for $P_{\mathrm{B}} = 1$ they are negative for all ρ. Therefore, the critical $P_{\mathrm{B4,c}}^{\mathrm{BKA}}$ is obtained when the determinant of the matrix equals zero, which yields

$$P_{\mathrm{B4,c}}^{\mathrm{BKA}} = 1 - \frac{4\rho^3}{9 - 3\rho^2}. \tag{C6}$$

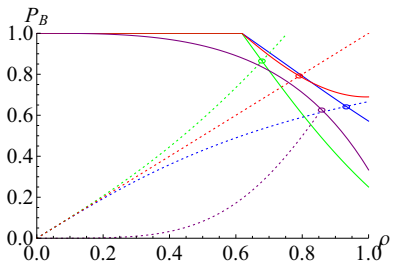

FIG. 25. The value of $P_{\mathrm{B,c}}$ (continuous lines) and $P_{\mathrm{B,ss}}$ (dotted lines) as a function of the density ρ for the DKA model (red), DAKA model (blue), DBKA model (green), and BKA model (purple). The small circles are the points at which the nontrivial solution ceases to exist.

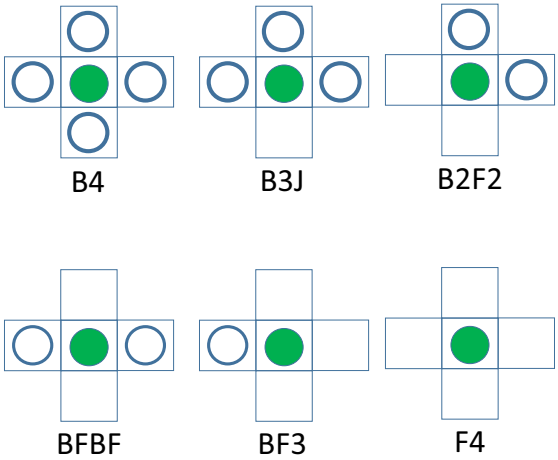

FIG. 26. An illustration of the six states of particles in the BKA model, up to symmetries.

For densities slightly below ρ_c, in which the nontrivial solution exists and is stable, the stationary value of P_{B} in the driven models is

$$P_{\mathrm{B,ss}} = \frac{\Omega_{\mathrm{F,B}} + \omega_{\mathrm{J,B}}}{\omega_{\mathrm{J,B}} + \omega_{\mathrm{B,J}} + \omega_{\mathrm{B,F}}}. \tag{C7}$$

In the BKA model we find it numerically. Figure 25 shows $P_{\mathrm{B,c}}$ and $P_{\mathrm{B,ss}}$ as a function of ρ for the four models DKA, DAKA, DBKA, and BKA. Note that in the DKA and DBKA models, but not in the DAKA and BKA models, there is a range of densities for which $P_{\mathrm{B,c}} < P_{\mathrm{B,ss}}$.

APPENDIX D: SMF APPROXIMATION IN THE BKA MODEL

In the BKA model there are six states illustrated in Fig. 26: B4 in which all the four nearest neighbors of the main particle are occupied, B3J in which three of the four nearest neighbors are occupied and the fourth is vacant, B2F2 in which two adjacent neighbors are occupied, BFBF in which two nonadjacent neighbors are occupied, BF3 in which one neighbor is occupied, and F4 in which all four neighbors are vacant. Since the sum of all six probabilities is 1, there are five coupled nonlinear equations. We numerically solve them in order to find the steady state.

1. Conditional probabilities

In the BKA model we are interested in the probability that a particle can move in a specific direction, P_{M}, the probability that it can move in a specific direction given that its neighbor in the opposite direction is occupied, $P_{\mathrm{M}|o}$, the probability that it can move in a specific direction given that its neighbor in the direction perpendicular to its motion is occupied, $P_{\mathrm{M}|s}$, the probability that it can move in a specific direction given that its neighbor in the direction perpendicular to its motion is vacant, $P_{\mathrm{M}|v}$, the probability that it can move in a specific direction given that the target site is vacant, $P_{\mathrm{M}|t}$, the probability that it can move in a specific direction given that its neighbor in the direction perpendicular to its motion is occupied and that the target site is vacant, $P_{\mathrm{M}|st}$, and the probability that it can move in a specific direction given that both its neighbor in the direction perpendicular to its motion and the target site are vacant, $P_{\mathrm{M}|vt}$. The probability P_{M} is

$$P_{\mathrm{M}} = \tfrac{1}{2}(P_{\mathrm{B2F2}} + P_{\mathrm{BFBF}}) + \tfrac{3}{4}P_{\mathrm{BF3}} + P_{\mathrm{F4}}. \tag{D1}$$

The conditional probability $P_{\mathrm{M}|o}$ is

$$P_{\mathrm{M}|o} = \frac{P_{\mathrm{M}\cap o}}{\rho} = \rho^{-1}(P_{\mathrm{B2F2}\cap \mathrm{o}} + P_{\mathrm{BF3}\cap \mathrm{o}}) = \rho^{-1}\left(\frac{1}{2}P_{\mathrm{B2F2}} + \frac{1}{4}P_{\mathrm{BF3}}\right). \tag{D2}$$

The conditional probability $P_{\mathrm{M}|s}$ is

$$P_{\mathrm{M}|s} = \frac{P_{\mathrm{M}\cap s}}{\rho} = \rho^{-1}(P_{\mathrm{B2F2}\cap \mathrm{s}} + P_{\mathrm{BFBF}\cap \mathrm{s}} + P_{\mathrm{BF3}\cap \mathrm{s}}) = \rho^{-1}\left(\frac{1}{4}P_{\mathrm{B2F2}} + \frac{1}{2}P_{\mathrm{BFBF}} + \frac{1}{4}P_{\mathrm{BF3}}\right). \tag{D3}$$

The conditional probability $P_{\mathrm{M}|v}$ is

$$P_{\mathrm{M}|v} = \frac{P_{\mathrm{M}\cap v}}{1-\rho} = (1-\rho)^{-1}(P_{\mathrm{B2F2}\cap \mathrm{v}} + P_{\mathrm{BF3}\cap \mathrm{v}} + P_{\mathrm{F4}\cap \mathrm{v}}) = (1-\rho)^{-1}\left(\frac{1}{4}P_{\mathrm{B2F2}} + \frac{1}{2}P_{\mathrm{BF3}} + P_{\mathrm{F4}}\right). \tag{D4}$$

The conditional probability $P_{\mathrm{M}|t}$ is

$$P_{\mathrm{M}|t} = \frac{P_{\mathrm{M}\cap t}}{1-\rho} = \frac{P_{\mathrm{M}}}{1-\rho}. \tag{D5}$$

The conditional probabilities $P_{\mathrm{M}|vt}$ and $P_{\mathrm{M}|st}$ are

$$\begin{aligned} P_{\mathrm{M}|vt} &= \frac{P_{\mathrm{M}\cap v\cap t}}{(1-\rho)^2} = \frac{P_{\mathrm{M}\cap v}}{(1-\rho)^2} = \frac{P_{\mathrm{M}|v}}{1-\rho}, \\ P_{\mathrm{M}|st} &= \frac{P_{\mathrm{M}\cap s\cap t}}{\rho(1-\rho)} = \frac{P_{\mathrm{M}\cap s}}{\rho(1-\rho)} = \frac{P_{\mathrm{M}|s}}{1-\rho}. \end{aligned} \tag{D6}$$

2. $r^{\mathrm{BKA}}_{\mathrm{B4,B3J}}$

This transition is illustrated in Fig. 27. At least one of the $\times$ sites is vacant. The rate is

$$r^{\mathrm{BKA}}_{\mathrm{B4,B3J}} = P_{\mathrm{M}|o} + 2P_{\mathrm{M}|s}. \tag{D7}$$

3. Outgoing rates from B3J

The outgoing rates from state B3J are illustrated in Fig. 28. In Figs. 28(a) and 28(b) at least one of the $\times$ sites is vacant, and in Figs. 28(c) and 28(d) the transition occur if the particle

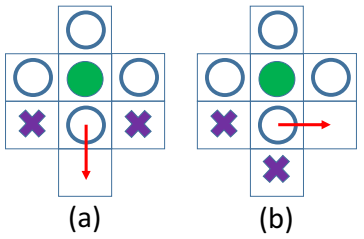

FIG. 27. An illustration of the transition B4 → B3J.

moves in one of the three directions. The rates are

$$r^{\mathrm{BKA}}_{\mathrm{B3J,B4}} = \tfrac{1}{4}(\rho P_{\mathrm{M}|t} + 2\rho P_{\mathrm{M}|st}),$$
$$r^{\mathrm{BKA}}_{\mathrm{B3J,B2F2}} = \tfrac{1}{4}(4P_{\mathrm{M}|s} + 2P_{\mathrm{M}|o}),$$
$$r^{\mathrm{BKA}}_{\mathrm{B3J,BFBF}} = \tfrac{1}{4}(2P_{\mathrm{M}|s} + P_{\mathrm{M}|o}). \quad \text{(D8)}$$

4. Outgoing rates from B2F2

The outgoing rates from state B2F2 are illustrated in Fig. 29. Figure 29(a) shows the transition induced by the main particle moving. The state after the move depends on the three sites marked ⋄. Figures 29(b)–29(d) show the transition to B3J induced by an incoming particle. Figure 29(e) shows the transition to BF3 induced by the movement of one of the blocking particles. The rates are

$$r^{\mathrm{BKA}}_{\mathrm{B2F2,B3J}} = \tfrac{1}{2}[\rho^3 + \rho P_{\mathrm{M}|t} + \rho P_{\mathrm{M}|vt} + \rho P_{\mathrm{M}|st}],$$
$$r^{\mathrm{BKA}}_{\mathrm{B2F2,BFBF}} = \tfrac{1}{2}\rho^2(1-\rho),$$
$$r^{\mathrm{BKA}}_{\mathrm{B2F2,BF3}} = \tfrac{1}{2}[3\rho(1-\rho)^2 + 2P_{\mathrm{M}|s} + P_{\mathrm{M}|o}],$$
$$r^{\mathrm{BKA}}_{\mathrm{B2F2,F4}} = \tfrac{1}{2}(1-\rho)^3. \quad \text{(D9)}$$

5. Outgoing rates from BFBF

The outgoing rates from state BFBF are illustrated in Fig. 30. Figure 30(a) shows the transition induced by the main particle moving. The state after the move depends on the three sites marked ⋄. Figures 30(b) and 30(c) show the transition to B3J induced by an incoming particle. Figure 30(d) shows the transition to BF3 induced by the movement of one of the blocking particles. The rates are

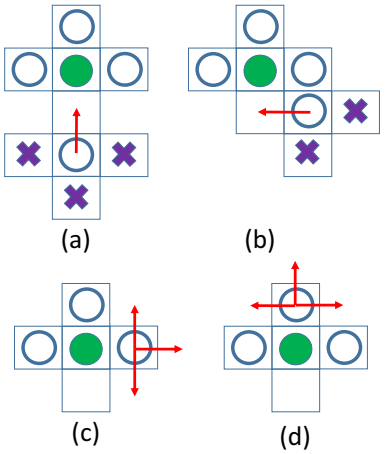

FIG. 28. An illustration of the outgoing transitions from B3J.

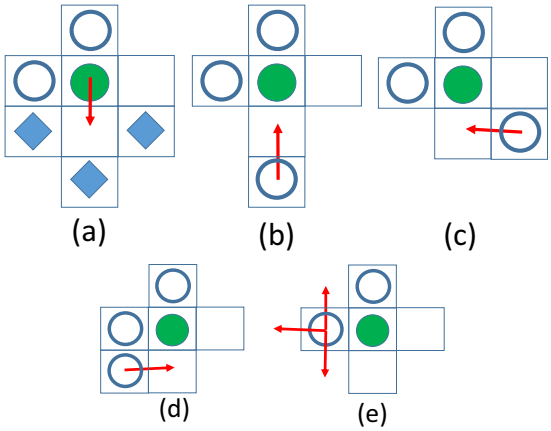

FIG. 29. An illustration of the outgoing transitions from B2F2.

$$r^{\mathrm{BKA}}_{\mathrm{BFBF,B3J}} = \tfrac{1}{2}(\rho^3 + \rho P_{\mathrm{M}|t} + 2\rho P_{\mathrm{M}|st}),$$
$$r^{\mathrm{BKA}}_{\mathrm{BFBF,B2F2}} = \rho^2(1-\rho),$$
$$r^{\mathrm{BKA}}_{\mathrm{BFBF,BF3}} = \tfrac{1}{2}[3\rho(1-\rho)^2 + 2P_{\mathrm{M}|s} + P_{\mathrm{M}|o}],$$
$$r^{\mathrm{BKA}}_{\mathrm{BFBF,F4}} = \tfrac{1}{2}(1-\rho)^3. \quad \text{(D10)}$$

6. Outgoing rates from BF3

The outgoing rates from state BF3 are illustrated in Fig. 31. Figure 31(a) shows the transition induced by the main particle moving in either of the three directions. The state after the move depends on the three sites marked ⋄. Figures 31(b)–31(d) show the transition to B2F2 induced by an incoming particle. Figures 31(e) and 31(f) show the transition to B2F2 induced by an incoming particle. Figure 31(g) shows the transition to F4 induced by the movement of one of the blocking particles. The rates are

$$r^{\mathrm{BKA}}_{\mathrm{BF3,B3J}} = \tfrac{3}{4}\rho^3,$$
$$r^{\mathrm{BKA}}_{\mathrm{BF3,B2F2}} = \tfrac{1}{2}[3\rho^2(1-\rho) + \rho P_{\mathrm{M}|t} + \rho P_{\mathrm{M}|st} + \rho P_{\mathrm{M}|vt}],$$
$$r^{\mathrm{BKA}}_{\mathrm{BF3,BFBF}} = \tfrac{1}{4}[3\rho^2(1-\rho) + 2\rho P_{\mathrm{M}|vt} + \rho P_{\mathrm{M}|t}],$$
$$r^{\mathrm{BKA}}_{\mathrm{BF3,F4}} = \tfrac{1}{4}[3(1-\rho)^3 + 2P_{\mathrm{M}|s} + P_{\mathrm{M}|o}]. \quad \text{(D11)}$$

7. Outgoing rates from F4

The outgoing rates from state F4 are illustrated in Fig. 32. Figure 32(a) shows the transition induced by the main particle

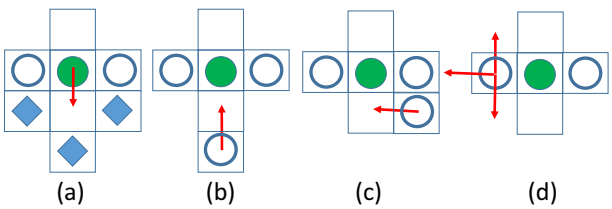

FIG. 30. An illustration of the outgoing transitions from BFBF.

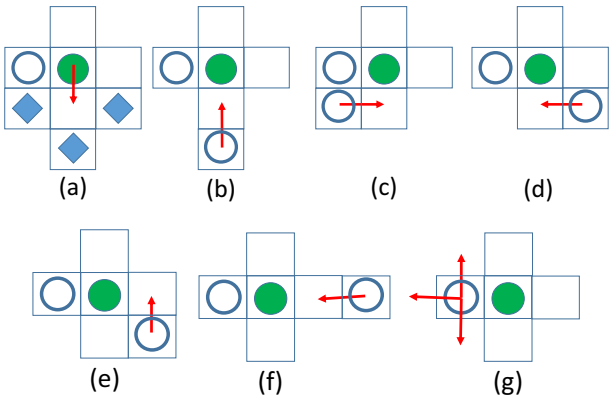

FIG. 31. An illustration of the outgoing transitions from BF3.

moving in either of the four directions. The state after the move depends on the three sites marked ⋄. Figures 32(b) and 32(c) shows the transition to BF3 induced by an incoming particle. The rates are

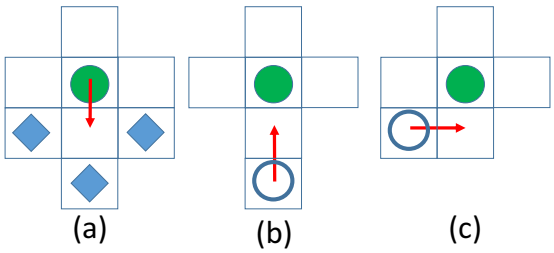

FIG. 32. An illustration of the outgoing transitions from F4.

$$
\begin{aligned}
r^{\mathrm{BKA}}_{\mathrm{F4,B3J}} &= \rho^3, \\
r^{\mathrm{BKA}}_{\mathrm{F4,B2F2}} &= 2\rho^2(1-\rho), \\
r^{\mathrm{BKA}}_{\mathrm{F4,BFBF}} &= \rho^2(1-\rho), \\
r^{\mathrm{BKA}}_{\mathrm{F4,BF3}} &= 3\rho(1-\rho)^2 + \rho P_{\mathrm{M}|t} + 2\rho P_{\mathrm{M}|vt}. \qquad \text{(D12)}
\end{aligned}
$$

[1] R. Durret, Ann. Probab. **12**, 999 (1984).
[2] D. Helbing, I. J. Farkas, and T. Vicsek, Nature (London) **407**, 487 (2000).
[3] D. R. Parisi and C. O. Dorso, *Pedestrian and Evacuation Dynamics*, edited by N. Waldau, P. Gattermann, H. Knoflacher, and M. Schreckenberg (Springer, Berlin, 2005) pp. 341-346.
[4] A. Garcimartin, I. Zuriguel, J. M. Pastor, C. Martin-Gomez, and D. R. Parisi, Transp. Res. Proc. **2**, 760 (2014).
[5] I. M. Sticco, F. E. Cornes, G. A. Frank, and C. O. Dorso, Phys. Rev. E **96**, 052303 (2017).
[6] J. M. Chen, P. Lin, F. Y. Wu, D. L. Gao, and G. Y. Wang, J. Stat. Mech. (2018) 023404.
[7] C. Gershenson and D. Helbing, Complexity **21**, 9 (2015).
[8] R. Tachet, P. Santi, S. Sobolevsky, L. I. Reyes-Castro, E. Frazzoli, D. Helbing, and C. Ratti, PLoS ONE **11**, e0149607 (2016).
[9] Y. Fily and M. C. Marchetti, Phys. Rev. Lett. **108**, 235702 (2012).
[10] G. S. Redner, M. F. Hagan, and A. Baskaran, Phys. Rev. Lett. **110**, 055701 (2013).
[11] M. Cates and J. Tailleur, Annu. Rev. Condens. Matter Phys. **6**, 219 (2015).
[12] L. F. Cugliandolo, P. Digregorio, G. Gonnella, and A. Suma, Phys. Rev. Lett. **119**, 268002 (2017).
[13] P. Digregorio, D. Levis, A. Suma, L. F. Cugliandolo, G. Gonnella, and I. Pagonabarraga, Phys. Rev. Lett. **121**, 098003 (2018).
[14] S. Whitelam, K. Klymko, and D. Mandal, J. Chem. Phys. **148**, 154902 (2018).
[15] J. U. Klamser, S. C. Kapfer, and W. Krauth, J. Chem. Phys. **150**, 144113 (2019).
[16] C. Merrigan, K. Ramola, R. Chatterjee, N. Segall, Y. Shokef, and B. Chakraborty, Phys. Rev. Research **2**, 013260 (2020).
[17] F. Spitzer, Adv. Math. **5**, 246 (1970).
[18] J. Jackle and A. Kronig, J. Phys.: Condens. Matter **6**, 7633 (1994).
[19] F. Ritort and P. Sollich, Adv. Phys. **52**, 219 (2003).
[20] C. Toninelli, G. Biroli, and D. S. Fisher, Phys. Rev. Lett. **96**, 035702 (2006).
[21] C. Toninelli and G. Biroli, J. Stat. Phys. **130**, 83 (2007).
[22] G. Biroli and C. Toninelli, Eur. Phys. J. B **64**, 567 (2008).
[23] M. Jeng and J. M. Schwarz, J. Stat. Phys. **131**, 575 (2008).
[24] M. Jeng and J. M. Schwarz, Phys. Rev. E **81**, 011134 (2010).
[25] J. Garrahan, P. Sollich, and C. Toninelli, *Dynamical Heterogeneities in Glasses, Colloids, and Granular Media*, International Series of Monographs on Physics (Oxford University Press, Oxford, 2010).
[26] A. Ghosh, E. Teomy, and Y. Shokef, Europhys. Lett. **106**, 16003 (2014).
[27] H. Ohta and S.-i. Sasa, J. Stat. Phys. **155**, 827 (2014).
[28] N. Segall, E. Teomy, and Y. Shokef, J. Stat. Mech. (2016) 054051.
[29] G. H. Fredrickson and H. C. Andersen, Phys. Rev. Lett. **53**, 1244 (1984).
[30] M. Sellitto, J. Phys. Condens. Matter **14**, 1455 (2002).
[31] G. Bolshak, R. Chatterjee, R. Lieberman, and Y. Shokef, Phys. Rev. E **100**, 032137 (2019).
[32] E. Teomy and Y. Shokef, Phys. Rev. E **95**, 022124 (2017).
[33] M. Sellitto, arXiv:cond-mat/9809186.
[34] M. Sellitto, Phys. Rev. E **65**, 020101(R) (2002).
[35] P. Gonçalves, C. Landim, and C. Toninelli, Ann. Inst. H. Poincaré Probab. Statist. **45**, 887 (2009).
[36] C. Arita, P. L. Krapivsky, and K. Mallick, J. Phys. A: Math. Theor. **51**, 125002 (2018).
[37] H. Hinrichsen, Adv. Phys. **49**, 815 (2000).
[38] Z. Racz, arXiv:cond-mat/0210435.
[39] G. Ódor, Rev. Mod. Phys. **76**, 663 (2004).
[40] B. Derrida, M. R. Evans, V. Hakim, and V. Pasquier, J. Phys. A: Math. Gen. **26**, 1493 (1993).
[41] M. Sellitto and J. J. Arenzon, Phys. Rev. E **62**, 7793 (2000).

[42] Y. Levin, J. J. Arenzon, and M. Sellitto, Europhys. Lett. **55**, 767 (2001).
[43] S. M. Fielding, Phys. Rev. E **66**, 016103 (2002).
[44] J. J. Arenzon, Y. Levin, and M. Sellitto, Physica A **325**, 371 (2003).
[45] H. C. Marques Fernandes, J. J. Arenzon, Y. Levin, and M. Sellitto, Physica A **327**, 94 (2003).
[46] M. Sellitto, Phys. Rev. Lett. **101**, 048301 (2008).
[47] Y. Shokef and A. J. Liu, Europhys. Lett. **90**, 26005 (2010).
[48] F. Turci, E. Pitard, and M. Sellitto, Phys. Rev. E **86**, 031112 (2012).
[49] W. Kob and H. C. Andersen, Phys. Rev. E **48**, 4364 (1993).
[50] E. Teomy and Y. Shokef, Phys. Rev. E **86**, 051133 (2012).
[51] E. Teomy and Y. Shokef, Phys. Rev. E **89**, 032204 (2014).
[52] C. Toninelli, G. Biroli, and D. S. Fisher, Phys. Rev. Lett. **92**, 185504 (2004).
[53] E. Teomy and Y. Shokef, J. Chem. Phys. **141**, 064110 (2014).
[54] A. E. Holroyd, Probab. Theory Relat. Fields **125**, 194 (2003).
[55] E. Teomy and Y. Shokef, Phys. Rev. E **92**, 032133 (2015).
[56] F. Corberi and L. F. Cugliandolo, J. Stat. Mech. (2009) P09015.